DocuServe

Electronic Delivery Cover Sheet

Caltech Library Services

International Journal of Infrared and Millimeter Waves, Vol. 1, No. 4, 1980

FAR INFRARED FINE STRUCTURE LINES IN THE INTERSTELLAR MEDIUM*

Dan M. Watson and J. W. V. Storey

Department of Physics
University of California
Berkeley, California 94720

Received May 14, 1980

Fine structure lines in the far-infrared have many simple properties that make them useful tools for diagnosing astrophysical plasmas. The line ratios are sensitive and accurate probes of density, elemental abundances, and ionization structure. In addition, studies of line shapes and Doppler shifts should prove valuable in studies of the gross dynamics of H II regions and galaxies. We present a review of the theory involved in the interpretation of these lines, and a summary of the observations made so far.

Key words: astronomy, fine structure lines, far-infrared spectroscopy.

Fine Structure Lines

Atomic and ionic fine structure lines are the infrared counterparts of the bright optical forbidden lines that have served astronomers for years as tools in the study of gaseous nebulae. These lines are produced by transitions within a multiplet of orbital angular momentum L, whose states of different total angular momentum J are split by the spin-orbit interaction. The energy that

*Work supported in part by NASA grant NGR 05-003-511.

0195-9271/80/1200-0609$03.00/0

fine structure lines carry away from gaseous nebulae comes from the kinetic energy of the gas, since the fine structure levels are populated by collisions. Along with the optical forbidden lines, which are also collisionally excited, atomic and ionic fine structure lines constitute the most important cooling mechanism in interstellar plasmas; in fact, they are the strongest lines in the far-infrared spectrum of ionized regions despite the low abundances of the atomic species that produce the lines.

In addition to carrying a lot of information on the emitting nebula, the far-infrared fine structure lines have simple observational properties that make it easy to extract that information. First, their wavelengths are long enough that the intensities are affected little by interstellar dust. In addition to obviating the need for reddening and absorption corrections, this property allows spectroscopic observations of invisible dust-shrouded regions. Second, nebulae are generally optically thin in fine structure lines (as is the case for optical forbidden lines and most recombination lines), so that no radiative transfer analysis is required. Third, most fine structure levels have excitation temperatures that are small compared to the ambient nebular temperature; this makes the fine structure line strengths relatively insensitive to nebular temperature. Fourth, for many ions the radiative rates (A coefficients) are sufficiently small that the collisional excitation and de-excitation rates are significantly larger even for quite low densities. Under these conditions the fine structure levels come into thermal equilibrium with the electrons, which because of the high electron temperatures involved, results in level populations dependent only on the statistical weights of states involved. This can occur even in very diffuse nebulae and results in a line intensity which is directly proportional to the ionic column density[13]. The ratios of the strengths of these "saturated" lines will yield very accurate relative abundances.

There is an additional useful property of ions that have more than one fine structure line: the ratio of the strengths of the two lines gives the electron density of the emitting region even when the region's size is unknown. This feature, which fine structure lines share with optical forbidden lines, makes the lines the most reliable indicators of electron density--other methods

depend upon knowing the depth of the nebula along the line of sight, which one can only guess at. However, meaningful results are obtained only when one of the pair of lines is not saturated.

The strongest fine structure lines will arise from ions that have fine structure in their ground-level multiplet. For ions of the more abundant elements, this means having a ^2P or ^3P ground-level multiplet--a property possessed by species with 1, 2, 4, or 5 p-electrons in their valence shell. Accordingly, we list the fine structure lines of the most abundant species in Table 1. Each of these lines should be detectable with present techniques (with the possible exception of the lines of silicon, which is highly depleted onto interstellar dust). Highly energetic ions , such as Ne^{++++}, have been omitted.

Atoms and ions that lack ground-state fine structure sometimes have fine structure in their next lowest-energy multiplet. These levels, though, are always so far above the ground-state as to make any fine structure emission very weak. The most promising examples are [O II]*, which has a line at 476 μm, and [S II], which has one at 317 μm. Both of these are well below present detection limits, however, so we will concern ourselves with ground-state fine structure lines for the time being.

For most of the lines in Table 1, detection in interstellar space has been the first direct measurement of their wavelength. The only laboratory technique with enough sensitivity to detect these lines is laser magnetic resonance (LMR). This technique depends on the paramagnetism of the studied species and a near-coincidence of the fine structure line frequency with that of a far-infrared laser. So far, the only lines that have yielded to such measurements are the [O I][8,39] and [C I][40] lines. For the lines not yet detected in interstellar space or measured in the laboratory, the wavelengths are calculated from energy level differences, derived from visible or ultraviolet spectral lines. The accuracy of

*The notation O I refers to allowed transition in the spectrum of neutral oxygen, O II to ionized oxygen (O^+), O III to O^{++}, and so on. Square brackets, such as [O III], denote forbidden transitions.

Table I - Important Infrared Fine Structure Lines

Transition	ION	λ(μm)	A(s^{-1})	Excitation Potential (eV)	Ionization Potential (eV)	Seen?
$2p:{}^2P_{3/2}-{}^2P_{1/2}$	C^+	157.4[15]	2.36×10^{-6}	11.260	24.383	yes
	N^{++}	57.30[47]	4.77×10^{-5}	29.601	47.448	yes
	O^{+++}	25.91	5.18×10^{-4}	54.934	77.413	yes
$3p:{}^2P_{3/2}-{}^2P_{1/2}$	Si^+	34.80	2.13×10^{-4}	8.151	16.345	no
	S^{+++}	10.52	7.70×10^{-3}	34.83	47.30	yes
$2p^2:{}^3P_1-{}^3P_0$	C^o	609.133[40]	7.93×10^{-8}	-	11.260	yes
${}^3P_2-{}^3P_1$		370.414[40]	2.68×10^{-7}			no
	N^+	203.9[12]	2.13×10^{-6}	14.534	27.601	no
		121.7[12]	7.48×10^{-6}			no

Table I - Important Infrared Fine Structure Lines (Cont'd)

Transition	ION	λ(μm)	A(s^{-1})	Excitation Potential (eV)	Ionization Potential (eV)	Seen?
	O^{++}	88.356[33]	2.62×10^{-5}	35.117	54.934	yes
		51.815[33]	9.75×10^{-5}			yes
$3p^2: {}^3P_1-{}^3P_0$	Si^{o}	129.68	8.25×10^{-6}	-	8.151	no
${}^3P_2-{}^3P_1$		68.474	4.20×10^{-5}			no
	S^{++}	33.443[12]	4.72×10^{-4}	23.33	34.83	yes
		18.713[4]	2.07×10^{-3}			yes
$2p^4: {}^3P_1-{}^3P_2$	O^{o}	63.170[39]	8.95×10^{-5}	-	13.618	yes
${}^3P_0-{}^3P_1$		145.526[8]	1.70×10^{-5}			no

Table I - Important Infrared Fine Structure Lines (Cont'd)

Transition	ION	λ(μm)	A(s^{-1})	Excitation Potential (eV)	Ionization Potential (eV)	Seen?
	Ne^{++}	15.55	5.99×10^{-3}	40.962	63.45	no
		36.04	1.15×10^{-3}			no
$3p^4:{}^3P_1-{}^3P_2$	S^{o}	25.246	1.40×10^{-3}	-	10.360	no
${}^3P_0-{}^3P_1$		56.322	3.02×10^{-4}			no
	Ar^{++}	8.99	3.08×10^{-2}	27.629	40.74	yes
		21.83	5.19×10^{-3}			no
$2p^5:{}^2P_{1/2}-{}^2P_{3/2}$	Ne^{+}	12.81	8.59×10^{-3}	21.564	40.962	yes
$3p^5:{}^2P_{1/2}-P_{3/2}$	Ar^{+}	6.99	5.26×10^{-3}	15.759	27.629	yes

far-infrared line wavelengths calculated in this manner is of the order of 1%. Many of the wavelengths listed in Table 1 are considerably more accurate than those in previous tabulations[35,42] since most of the transitions have only recently been directly measured. Unless otherwise indicated, the wavelengths have been obtained from the energy-level compilation of Bashkin and Stoner.[6] A new tabulation of important ionic energy levels and fine structure transition wavelengths is also currently in preparation by Greenberg and Kaufman.[14] The A-coefficients are from Wiese et al.,[48] and the excitation potentials and ionization potentials from Moore.[30]

Theory

The quantities measured most accurately by fine structure line intensities are electron density and relative ionic abundances. The fairly simple means for deriving these parameters from the observed intensities is outlined in this section.

The power per unit area and solid angle emitted in a fine structure line can be expressed by the usual formula for optically thin emission:

$$I_{kj} = \frac{h\nu}{4\pi} A_{kj} \, n_k \ell \qquad (1)$$

where A_{kj} is the Einstein A-coefficient of the transition $k \rightarrow j$, ν is the line frequency, and $n_k \ell$ is the column density in the k^{th} state, averaged over the beam and the line of sight:

$$n_k \ell \equiv \frac{1}{\Delta\Omega} \int_{\Delta\Omega} d\Omega \int_0^{\ell} dr \, n_k(r, \Omega) \qquad (2)$$

For ionized species, excitation of the fine structure levels is due mostly to electron collisions. We can relate the density n_k to the electron density n_e and the ionic fractional abundance F by

$$n_k = \frac{f_k}{\sum_j f_j} F n_e$$

where f_j is the fractional population of the state j relative to the ground state. The f's can be calculated by using the principle of detailed balance. Since absorption and stimulated emission are negligible, we have

$$f_j \left[\sum_k n_e \gamma_{jk} + \sum_{k<j} A_{jk} \right] = \sum_k f_k n_e \gamma_{kj} + \sum_{k>j} f_k A_{kj} \qquad (3)$$

where γ_{kj} is the collisional rate coefficient for the transition k→j, as discussed in Appendix A. For the densities normally encountered in the interstellar medium, nearly all of the ions will be in the ground term. For the case of ground-term fine structure lines, then, (3) reduces to a system of one or two independent equations depending upon whether the ion has a doublet or triplet ground term. The solutions of (3) for both cases are given in Appendix B. For the O^{++} species, (3) yields values of f_k that are plotted in Figure 1.[43] Note that the dependence on temperature is weak, a result of the close spacing of the fine structure energy levels.

As we mentioned in the previous section, the fine structure levels come to thermal equilibrium ("saturate") at very low densities. This is expressed in Figure 1, which shows that the [O III] fine structure lines are fully saturated at densities of 10^3-10^4 cm^{-3} (compared to $\sim 10^5$-10^6 for the optical forbidden lines of [O III]). With the states in thermal equilibrium being populated according to their statistical weights, the $f_k / \sum_j f_j$ are constant, and the line intensity is proportional to the total ionic column density $n_{ion}\,\ell$. (At densities much lower than the thermal equilibrium density, the line intensity will be proportional to $n_{ion}\, n_e\, \ell$, just as in the case of recombination lines.) Comparison of intensities of the saturated lines will thus give accurate relative abundances; the more closely saturation is approached the less will be the uncertainty in abundance. In most cases, abundances derived in this way will be considerably more accurate than determinations from optical lines.

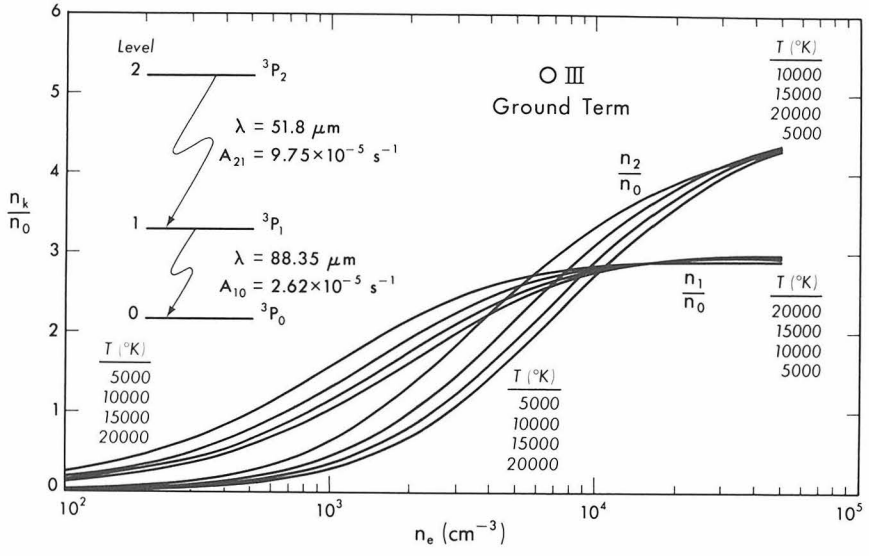

Figure 1. O^{++} fine structure level population ratios.

Ions that have ^3P ground terms, like O^{++}, have two fine structure lines. If the intensity of each line is measured in the same beam and along the same line of sight, Equation (1) may be written twice to give equations in the unknowns n_e and F. These can be solved for the electron density, independent of the length of the emitting region:

$$n_e = \frac{\gamma_{01}(A_{21}+A_{20}) + \gamma_{02}(A_{21} - \frac{R}{a} A_{10})}{\gamma_{01}\left(\frac{R}{a}\gamma_{12}-\gamma_{21}-\gamma_{20}\right) + \gamma_{02}\left[\frac{R}{a}(\gamma_{12}+\gamma_{10})-\gamma_{21}\right]} \qquad (4)$$

where the subscripts 0, 1, 2 label the states of the fine structure triplet in order of increasing energy, and where $R \equiv I_{10}/I_{21}$ and $a \equiv \lambda_{21}A_{10}/\lambda_{10}A_{21}$. Substituting the derived value of n_e back into Equation 1, along with values for ℓ and $\Delta\Omega$, gives the other unknown, the ionic abundance

F. This last step usually requires assumptions about the depth and shape of the nebula along the line of sight, so the ionic abundances relative to hydrogen derived in this fashion may not be as accurate as ion-ion relative abundances.

The most important uses of the quantities derived from far-infrared fine structure line intensities include the study of energy balance in gaseous nebulae, general elemental abundances and ionization structure of H II regions. For instance, the ionization structure of a nebula may be obtained as follows. Once the electron density has been determined at all points within the nebula, the flux of ionizing photons Φ can be obtained by equating the rate at which hydrogen atoms are ionized to the rate at which the resulting hydrogen ions recombine with electrons. Since every ionizing photon will be eventually absorbed in the nebula, the left hand side of this equation is just Φ. The right hand side will be the integral over space of the recombination rate coefficient, times the product of n_e and n_{H^+}. Note that $n_e = n_{H^+}$, since hydrogen is overwhelmingly the most abundant element. Thus

$$\Phi = \int n_e^2 \, \alpha_B(H^o) \, dV \qquad (5)$$

where $\alpha_B(H^o)$ is the recombination rate coefficient into all states of neutral hydrogen except the ground state. If the source of ionizing radiation is centralized, the intensity of ionizing flux decreases with $1/R^2$. The recombination rate is directly proportional to electron density. Therefore the population of any ionized state depends upon $\Phi/n_e R^2$. One can calculate the fractional abundances of ions as a function of $\Phi/n_e R^2$ by solving the equations of photoionization equilibrium:

$$n(x^i) \int_{\nu_i}^{\infty} \frac{4\pi J_\nu}{h\nu} \sigma_\nu(x^i) d\nu = (x^{i+1}) n_e \alpha(x^i, T) \qquad (6)$$

Here $n(x^i)$ is the density of element x in the ionization state i; $\alpha(x^i,T)$ is the recombination rate coefficient, in $cm^3\ s^{-1}$, of the species x^i; n_e is the free electron

density; $\sigma_\nu(x^i)$ is the photoionization cross section of x^i, $h\nu_i$ is the ionization potential of x^i, and J_ν is the mean intensity of radiation (energy per unit time, area, and frequency interval averaged over solid angle). The procedure is discussed in standard textbooks (Osterbrock,[34] for instance). We show the results of such a calculation, for oxygen, in Figure 2.

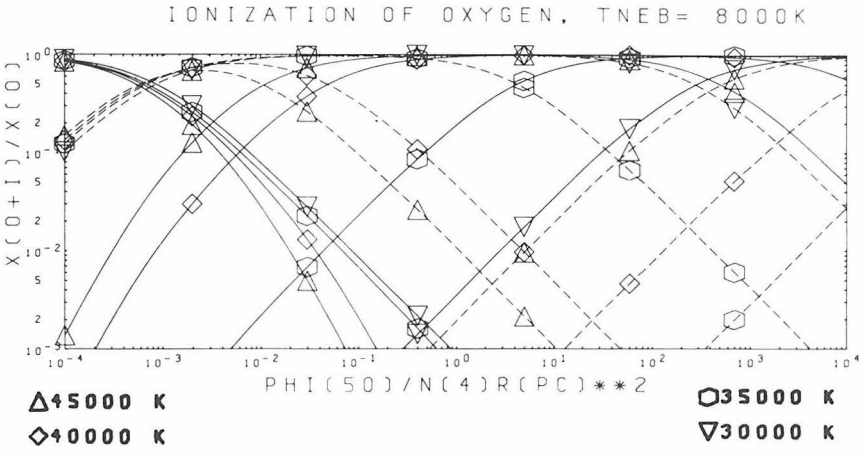

Figure 2. Population ratios of the ionization states of oxygen for various values of stellar temperature, as functions of $\Phi_{50}/n_4 R^2_{pc}$. Here Φ_{50} is the flux of the hydrogen-ionizing photons, in units of 10^{50} photons s^{-1}; n_4 is the nebular electron density, in units of 10^4 cm^{-3}; and R_{pc} is the mean radius of the nebula in parsecs (1pc = 3.09 x 10^{18} cm). The two families of solid curves represent the fractional populations of O^o (leftmost family) and O^{++}; the dashed curves are for O^+ (leftmost family of dashed curves) and O^{+++}. Model stellar atmospheres with solar abundances of heavy elements and surface gravity log g = 5 have been used in the calculations.[19]

By measuring F and n_e from fine-structure line ratios and plotting the appropriate point on Figure 2, the effective temperature of the ionizing star can be determined.

This information can be of considerable interest, particularly if the star in question is completely obscured from view by interstellar dust.

Observations

The first fine structure lines to be detected were the [Ne II] 12.81 μm, [S IV] 10.52 μm, and [Ar III] 8.99 μm lines, which lie in the 8-14 μm atmospheric window. These lines have been studied extensively by several groups and will not be reviewed here; we will restrict our domain to wavelengths of 18 μm and greater, on out into the submillimeter. In this region, only two lines fall in atmospheric windows. One of these, the [S III] 18.71 μm line, was discovered during ground-based observations,[13] but was found to be so close to an atmospheric water vapor absorption line that airborne observations are advantageous. The other, [C I] 370.41 μm, has not yet been detected.

Airborne spectroscopic observations have been made from three platforms: the NASA Lear Jet, with a 30 cm telescope; the NASA Kuiper Airborne Observatory, a Lockheed C-141 with a 91 cm telescope; and the University College London balloon-borne observatory, with a 60 cm telescope. Several research groups with their own focal plane instruments have reported observations of fine structure lines with these telescopes: (a) The group at Cornell University has two grating-photoconductor systems, one for 40 μm-200 μm[16] and one for 18-40 μm.[25] The former system, flown on the Lear Jet, has been used in the first detections of [O III] 88.35 μm,[45] [O III] 51.81 μm,[28] [O I] 63.17 μm,[26] and most recently [C II] 157.4 μm.[15] Further observations have been carried out with this instrument on both the Lear Jet and the C141.[7,27,29] The 18-40 μm system has so far been used on the Lear Jet for observations of [S III] 18.71 μm,[25] and on the C141 for the detection of [Ne V] 24.28 μm and [O IV] 25.91 μm.[11] (b) Two European collaborations (ESA, Observatoire de Meudon and Laboratoire de Physique Stellaire et Planetaire on the C141;[3] ESA/UCL on the UCL balloon-borne telescope) have used Michelson interferometer-bolometer systems to detect [N III] 57.30 μm[33] and [S III] 33.44 μm,[32] as well as further observations of these lines, the two

[O III] lines, [S III] 18.71 μm, and [O I] 63.17 μm.[1,4,5,31,32,33]

(c) The Bell Laboratories InSb hot-electron photoconductor heterodyne receiver, long used for submillimeter- and millimeter-wave molecular line observations, has recently been used on the C141 to detect [C I] 609.1 μm.[36]

(c) At the University of California, Berkeley, a tandem Fabry-Perot photoconductor system, described in a companion paper,[44] has been used to observe [O III] 51.8 μm,[46,47] and 88.35 μm,[43] [N III] 57.30 μm,[47] and [O I] 63.17 μm.[43] This work has produced the first maps of H II regions in these fine structure lines.

(e) Nearing completion is the tandem Fabry-Perot-bolometer system developed by a group at CNRS[23] for use on the Smithsonian Astrophysical Observatory's balloon-borne observatory. It will be used primarily for the [C II] 157.4 μm line. Also, the group at Imperial College[17] have essentially completed a liquid nitrogen-cooled Fabry-Perot spectrometer for use on their 41" balloon-borne telescope.

A summary of observations made to date by all of the groups discussed above is presented in Table 2. We have omitted the [S III] 33.44 μm line which has been detected only in M17[32] and also the [O IV] 25.91 μm and [Ne V] 24.28 μm lines which have been detected only in NGC7027.[11]

So far, no studies have been made of the velocity structure of these lines. The spectral resolution of existing instruments is already sufficient to provide limited velocity information, but future instrumental developments--particularly the extension of heterodyne techniques to the far-infrared--will enable detailed studies of the dynamics and expansion of H II regions at various stages throughout their evolution.

Acknowledgments

We gratefully acknowledge helpful discussions with C.H. Townes. We also thank the many authors who have informed us of their results prior to publication.

Table II - Summary of Observations

Source	[S III] 18.17μm	[O III] 51.81μm	[N III] 57.30μm	[O I] 63.17μm	[O III] 88.35μm	[C II] 157.4μm	[C I] 609.1μm
Sgr A		46			7		
M42	4,25,31	27,28		26,43	4,7,43,31	15	36
M17	25,32	27,33,32,47	33,32,47	26,43	7,43,45,33,32		
M8		5			7		
NGC7538	5	47,5			43,5		
NGC7027	13			29			
NGC6543		47					
NGC6357		27,33		33	7,33		
NGC6334					33		
NGC2264							36
NGC2024	25					15	36
W51	25	27,33,47	33,47		33,43		36

Table II - Summary of Observations (Cont'd)

Source	[S III] 18.71μm	[O III] 51.81μm	[N III] 57.30μm	[O I] 63.17μm	[O III] 88.35μm	[C II] 157.4μm	[C I] 609.1μm
W49	5	47,5			43,5		
W43		47					
W3	31				7,43		36
G333.6-0.2	13	33			33		
S140							36
BD $30^{\circ}3639$	13						
DR21				43			

Appendix A

The collisional rate coefficient γ_{kj} for the transition state k to lower-energy state j is given by

$$\gamma_{kj} = \frac{h^2 \Omega_{jk}}{g_k (2\pi m_e)^{3/2} (kT)^{1/2}} = \frac{8.629 \times 10^{-6} \Omega_{jk}}{g_k T^{1/2}} \qquad (A1)$$

and the rate for the reverse process is

$$\gamma_{jk} = \frac{g_k}{g_j} \gamma_{kj} \quad e^{-(E_k - E_j)/kT} \qquad (A2)$$

where g_i is the degeneracy of state i, and T is the kinetic temperature. Ω_{jk} is a dimensionless parameter called the collision strength, given by:

$$\Omega_{jk} = \frac{2 g_j m_e}{\pi h^2 kT} \int_0^\infty dE \; E e^{-E/kT} \sigma_{jk}(E) \qquad (A3)$$

where $\sigma_{jk}(E)$ is the cross section for the collisionally-induced transition, given as a function of energy of the incoming particle. The collision strengths turn out to be fairly insensitive to temperature in the case of electron collisional excitation of ions, so that the temperature dependence of the downward collision rate (A1) is essentially $T^{-1/2}$.

For ions with excitation potentials greater than the ionization potential of hydrogen, the dominant form of excitation will be collisions with free electrons. The calculation of electron collision strengths is discussed by Saraph, Seaton, and Shemming[38] and by Krueger and Czyzak;[18] these authors also tabulate results for $2p^n$ and $3p^n$ electron configurations. Improved calculations frequently appear in the literature.[41]

Neutral species and singly-ionized species with excitation potentials less than the ionization potential of hydrogen usually lie in regions where collisions with hydrogen atoms and hydrogen molecules (and perhaps helium atoms) are the dominant excitation processes. Calculations of the relevant collision strengths are rare. For the important ion C^+, calculations of collisions with neutral atomic hydrogen[21] and molecular hydrogen[9,10] show that the C^+-H^o and C^+-H_2 collision strengths are nearly equal. Collision strengths for C^o-H^o are also available.[22] Further results in this area would be welcome, especially collision strengths for neutral carbon and sulfur. Proton collision strengths for sulfur have recently been calculated.[20]

Neutral oxygen is peculiar in that its ionization potential (13.618 eV) is very close to that of hydrogen (13.598 eV); significant [O I] emission can thus arise from both the ionized and neutral sides of ionization fronts. One must therefore consider collisions with hydrogen atoms[22] as well as electrons;[24,37] furthermore, the charge neutrality of O^0 eliminates the "focussing" effect that makes electron collisions much more important than proton collisions for fine structure excitation of ions, and proton collisions must be included.[2,20] The results of a calculation of the O^o fine structure level populations, using the calculated e^- - O^o, p - O^o, and H^o - O^o collision strengths, is presented in Storey et al.[43]

Appendix B - Population Ratios

If the fine structure levels are labelled 0, 1, 2 in order of increasing energy, the solutions to the detailed balance equation (3) are

$$f_1 = \frac{n_e\gamma_{01}}{n_e\gamma_{10}+A_{10}} \tag{B1}$$

for ground-term doublets (p^1 and p^5 configurations), and

$$f_1 = \frac{\left[n_e\gamma_{01}+\frac{\gamma_{02}}{\gamma_{12}}\left[n_e(\gamma_{12}+\gamma_{10})+A_{10}\right]\right]\left[n_e(\gamma_{21}+\gamma_{20})+A_{21}+A_{20}\right]}{\left[n_e(\gamma_{21}+\gamma_{20})+A_{21}+A_{20}\right]\left[n_e(\gamma_{12}+\gamma_{10})+A_{10}\right]-n_e\gamma_{12}(n_e\gamma_{21}-A_{21})} - \frac{\gamma_{02}}{\gamma_{12}} \tag{B2}$$

$$f_2 = \frac{n_e\gamma_{12}\left[n_e\gamma_{01}+\frac{\gamma_{02}}{\gamma_{12}}\left[n_e(\gamma_{12}+\gamma_{10})+A_{10}\right]\right]}{\left[n_e(\gamma_{21}+\gamma_{20})+A_{21}+A_{20}\right]\left[n_e(\gamma_{12}+\gamma_{10})+A_{10}\right]-n_e\gamma_{12}(n_e\gamma_{21}+A_{21})} \tag{B3}$$

for ground-term triplets (p^2 and p^4 configurations).

References

[1]M. Anderegg, A.F.M. Moorwood, P. Salinari, I. Furniss, R.E. Jennings, K.J. King, W.A. Towlson, and T.E. Venis, Astron.Astrophys. 82, 86 (1980).

[2]J.N. Bahcall and R.A. Wolf, Astrophys.J. 152, 701 (1968).

[3]J.P. Baluteau, M. Anderegg, A.F.M. Moorwood, N. Coron, J.E. Beckman, E. Bussoletti, and H.H. Hippelein, Appl. Opt. 16, 1834 (1977).

[4]J.P. Baluteau, E. Bussoletti, M. Anderegg, A.F.M. Moorwood, and N. Coron, Astrophys.J.Lett. 210, L45 (1976).

[5]J.P. Baluteau, A.F.M. Moorwood, Y. Biraud, N. Coron, M. Anderegg, and B. Fitton, (submitted to Astrophys.J. 1980).

[6]S. Bashkin and J.B. Stoner, Jr., Atomic Energy Levels and Grotrian Diagrams North-Holland, Amsterdam, V. 1 (1975) and V.2 (1978).

[7]F.W. Dain, G.E. Gull, G. Melnick, M. Harwit, and D.B. Ward, Astrophys.J.Lett. 221, L17 (1978).

[8]P.B. Davies, B.J. Handy, E.K. Murray Lloyd, and D.R. Smith, J.Chem.Phys. 68, 1135 (1978).

[9]D.R. Flower and J.M. Launay, J.Phys.B. 10, L229 (1977).

[10]D.R. Flower and J.M. Launay, J.Phys.B. 10, 3673 (1977).

[11]W.J. Forrest, J.F. McCarthy, and J.R. Houck, Astrophys. J.Lett. (to be published 1980).

[12]L.T. Greenberg, Personal Communication (1980).

[13]L.T. Greenberg, P. Dyal, and T.R. Geballe, Astrophys.J. Lett. 213, L71 (1977).

[14]L.T. Greenberg and V. Kaufman (in preparation 1980).

[15]M. Harwit, Personal Communication (1979).

[16]J.R. Houck and D.B. Ward, Publ.Astron.Soc.Pac. 91, 140 (1979).

[17]R.D. Joseph, Personal Communication (1980).

[18]T.K. Krueger and S.J. Czyzak, Proc.R.Soc.A, 318, 531 (1970).

[19]R.L. Kurucz, Astrophys.J.Suppl.Ser. 40, 1 (1979).

[20]D. Landman, (submitted to Astrophys.J. 1980).

[21]J.M. Launay and E. Roueff, J.Phys.B. 10, 879 (1977).

[22]J.M. Launay and E. Roueff, Astron.Astrophys. 56, 289 (1977).

[23]J.C. Lecullier and G. Chanin, Infrared Phys. 16, 273 (1976).

[24]M. LeDourneff and R.K. Nesbet, J.Phys. B. 9, L241 (1976).

[25]J.F. McCarthy, W.J. Forrest, and J.R. Houck, Astrophys. J. 231, 711 (1979).

[26]G. Melnick, G.E. Gull, and M. Harwit, Astrophys.J.Lett. 227, L29 (1979).

[27]G. Melnick, G.E. Gull, and M. Harwit, Astrophys.J.Lett. 227, L35 (1979).

[28]G. Melnick, G.E. Gull, M. Harwit, and D.B. Ward, Astrophys.J.Lett. 222, L137 (1978).

[29]G. Melnick, R.W. Russell, G.E. Gull, and M. Harwit, Astrophys.J.Lett. (to be published 1980).

[30]C.E. Moore, Atomic Energy Levels, NSRDS - NBS 35 (1971).

[31]A.F.M. Moorwood, J.P. Baluteau, M. Anderegg, N. Coron, and Y. Biraud, Astrophys.J. 224, 101 (1978).

[32]A.F.M. Moorwood, J.P. Baluteau, M. Anderegg, N. Coron, Y. Biraud, and B. Fitton, Astrophys.J. (to be published 1980).

[33]A.F.M. Moorwood, P. Salinari, I. Furniss, R.E. Jennings, and K.J. King, (submitted to Astron.Astrophys. 1980)

[34]D.E. Osterbrock, Astrophysics of Gaseous Nebulae, (W.H. Freeman, San Francisco) (1974).

[35]V. Petrosian, Astrophys.J. 159, 833 (1970).

[36]T.G. Phillips, P.J. Huggins, T.B.H. Kuiper, and R.E. Miller (to be published, Astrophys.J.Lett. 239 (1980)).

[37]H.E. Saraph, J.Phys.B. 6, L243 (1973).

[38]H.E. Saraph, M.J. Seaton, and J. Shemming, Philos.Trans. R.Soc.Lond. A, 264, 77 (1969).

[39]R.J. Saykally and K.M. Evenson, J.Chem.Phys. 71, 1564 (1979).

[40]R.J. Saykally and K.M. Evenson, (to be published, Astrophys.J.Lett. 239 (1980)).

[41]M.J. Seaton, Mon.Not.R.Astron.Soc. 170, 475 (1975).

[42]J.P. Simpson, Astron.Astrophys. 39, 43 (1975).

[43]J.W.V. Storey, D.M. Watson, and C.H. Townes, Astrophys. J. 233, 109 (1979).

[44]J.W.V. Storey, D.M. Watson, and C.H. Townes, Int.J.IR and MM Waves, 1, 15 (1980).

[45]D.B. Ward, B. Dennison, G. Gull, and M. Harwit, Astrophys.J.Lett. 202, L31 (1975).

[46]D.M. Watson, J.W.V. Storey, C.H. Townes, and E.E. Haller, (submitted to Astrophys.J.Lett. 1980a).

[47]D.M. Watson, J.W.V. Storey, C.H. Townes, and E.E. Haller, (in preparation 1980b).

[48]W.L. Wiese, M.W. Smith, B.M. Glennon, Atomic Transition Probabilities (NSRDS-NBS4) (1966).